Alternate materials for the capture and quantification of gaseous oxidized mercury in the atmosphere

Livia Lown[1], Sarrah M. Dunham-Cheatham[2], Seth N. Lyman[3, 4], Mae S. Gustin[1]

[1]Department of Natural Resources and Environmental Science, University of Nevada, Reno, Reno, NV, 89557, USA
[2]College of Agriculture, Biotechnology & Natural Resources, University of Nevada, Reno, Reno, NV, 89557, USA
[3]Bingham Research Center, Utah State University, Vernal, UT, 84078, USA
[4]Department of Chemistry and Biochemistry, Utah State University, Logan, UT 84322, USA

Correspondence to: Mae S. Gustin (mgustin@unr.edu)

Abstract. Methodologies for identifying atmospheric oxidized mercury (Hg^{II}) compounds, including particulate-bound Hg^{II} ($Hg^{II}_{(p)}$) and gaseous oxidized mercury ($Hg^{II}_{(g)}$), by mass spectrometry (MS) are currently under development. This method requires preconcentration of Hg^{II} for analysis due to high instrument detection limits relative to ambient Hg^{II} concentrations. The objective of this work was to identify and test materials for quantitative capture of Hg^{II} from the gas phase, and to suggest potential surfaces onto which Hg^{II} can be collected, thermally desorbed, and characterized using MS methods. From the literature, several compounds were identified as potential sorbent materials and tested in the laboratory for uptake of gaseous elemental mercury (Hg^0) and $Hg^{II}_{(g)}$ (permeated from a $HgBr_2$ salt source). Chitosan, α-Al_2O_3, and γ-Al_2O_3 demonstrated $Hg^{II}_{(g)}$ capture in ambient air laboratory tests, without sorbing Hg^0 under the same conditions. When compared to cation exchange membranes (CEM), chitosan captured a comparable quantity of $Hg^{II}_{(g)}$, while $\leq 90\%$ of loaded $Hg^{II}_{(g)}$ was recovered from α-Al_2O_3, and γ-Al_2O_3. When deployed in the field, the capture efficiency of chitosan decreased compared to CEM, indicating environmental conditions impacted the sorption efficiency of this material. The poor recovery of Hg^{II} from the tested materials compared to CEM in the field indicate that further identification and exploration of alternative sorbent materials is required to advance atmospheric mercury chemistry analysis by MS methods.

1 Introduction

Mercury (Hg) is a toxic global contaminant that is introduced to aquatic and terrestrial ecosystems primarily from the atmosphere (Driscoll et al., 2013). Oxidized forms (Hg^{II}), including gaseous oxidized mercury ($Hg^{II}_{(g)}$) and particulate-bound mercury ($Hg^{II}_{(p)}$), are deposited from the atmosphere to ecosystems (Ariya et al., 2015), and may become available for transformation to and accumulation as methylmercury in food webs (Lyman et al., 2020a). A complete understanding of Hg behavior in the atmosphere is necessary to describe the fate of anthropogenic Hg pollution, assess health risks to humans and wildlife, and evaluate the effectiveness of the Minamata Convention. The mechanisms that govern the oxidation and reduction of Hg in the atmosphere are not well understood (Shah et al., 2021), and model results are uncertain, because they do not consider other forms of Hg^{II} present (Gustin et al., 2023).

For example, Shah et al. (2021) assumed all Hg^{II} compounds devolatilized from aerosols are $HgCl_2$. This is an assumption that has not been validated.

Currently, Br^- and Cl^- radicals are considered to participate in elemental Hg (Hg^0) oxidation. This is based on both theoretical work (Holms et al., 2010; Horowitz et al., 2017; Song et al., 2024) and experimental observations of atmospheric Hg depletion events in the Arctic (Steffen et al., 2008), as well as observations of Hg^{II} formation at the marine boundary layer (Laurier et al., 2003). The identity of $Hg^{II}_{(g)}$ compounds in the atmosphere is currently unknown, but mass spectrometry (MS) methods capable of observing atmospheric $Hg^{II}_{(g)}$ speciation are in development (cf., Jones et al., 2016; Khalizov et al., 2020; Mao and Khalizov, 2021). These methods have been developed using $HgBr_2$ and $HgCl_2$ as model atmospheric $Hg^{II}_{(g)}$ compounds, given the role of halogen radicals in atmospheric Hg^0 oxidation. However, due to differences in $Hg^{II}_{(g)}$ behavior, the use of a broad range of representative compounds is desirable in both MS method development and validation of preconcentration surfaces.

~~p~~ MS methods will require preconcentration of ambient $Hg^{II}_{(g)}$ for detection, but the preconcentration surfaces currently available for deployment in the field ha~~ves associated~~ve limitations which prevent their use in MS methods. Commonly used materials include potassium chloride (KCl)-coated denuders in the Tekran 2537/1130/1135 speciation system (Landis et al., 2002) and membranes deployed in the Reactive Mercury Active System (RMAS) (Luippold et al., 2020b). ~~Membranes used in the RMAS have included:~~These membranes include cation exchange membranes (CEM), used for quantitative Hg^{II} measurement; polytetrafluoroethylene membranes (PTFE), used to quantify $Hg^{II}_{(p)}$ (described in Luippold et al., 2020b as PBM); and nylon membranes, used for estimating Hg chemistry.

KCl denuders do not accurately measure Hg^{II} in ambient air due to ozone, humidity, and perhaps other interferences (Lyman et al., 2012; McClure et al., 2013; Huang et al., 2015). PTFE membranes exposed to field conditions have also recently been found to sorb $Hg^{II}_{(g)}$, indicating this membrane type cannot fully separate $Hg^{II}_{(g)}$ and $Hg^{II}_{(p)}$ measurements as intended, and provide $Hg^{II}_{(p)}$ measurements that are biased high (Allen et al., 2024). Although CEM outperform KCl denuders for quantitative $Hg^{II}_{(g)}$ capture (Huang et al., 2013), and are quantitative $Hg^{II}_{(g)}$ sorbants under laboratory conditions (Miller et al., 2019, Dunham-Cheatham 2020), recent work suggests CEM may not be fully quantitative under field conditions. For instance, Dunham-Cheatham et al. (2023) observed lower Hg^{II} concentrations collected on CEM (discussed as RM by Dunham-Cheatham et al. (2023)~~)~~, which includes $Hg^{II}_{(g)}$ and $Hg^{II}_{(p)}$ as defined here) in the field relative to co-located dual-channel system (DCS) $Hg^{II}_{(g)}$ measurements. However, it is possible that the discrepancy between CEM and DCS measurements observed by Dunham-Cheatham et al. (2023) was due to the 2 L min^{-1} flow rate used to collect Hg^{II} on CEM. Use of 2 L min^{-1} flow rates have recently been found to decrease Hg capture efficiency relative to those sampled at a 1 L min^{-1} flow rate (Allen et al., 2024). ~~Also, i~~Increased breakthrough has been detected on downstream CEM during field campaigns compared to CEM exposed to $Hg^{II}_{(g)}$ for short periods in the laboratory (Allen et al., 2024, and this work), and Hg^{II} loss from CEM during long campaign periods has yet to be quantified. CEM are not appropriate for Hg^{II} sample introduction into MS systems, for when heated they generate compounds that interfere with Hg quantification by cold vapor atomic absorption spectroscopy (Gustin et al., 2019), and research done using high Hg^{II} concentrations has suggested that exchange reactions can occur with Hg compounds on the CEM surface (Mao and Khalizov, 2021).

~~Current Hg^{II} measurement methods do not offer compound-level identification of the Hg compounds present (Luippold et al., 2020a).~~ Thermal desorption followed by peak deconvolution of Hg^{II} compounds from nylon membranes deployed in the RMAS is currently the only method available for estimating atmospheric Hg^{II} chemistry (Huang et al., 2013; Luippold et al., 2020a; Gustin et al., 2023). This method compares thermal desorption profiles of unknown Hg^{II} compounds to reference profiles developed from Hg^{II} salts permeated onto nylon membranes to identify potential compound constituents (e.g., -O, -Br/Cl, -N, -S, and –organic Hg compounds). The validity of thermal desorption interpretations depends on how well the desorption behavior of Hg salts represents unknown atmospheric Hg^{II} compounds. Exchange reactions involving HgBr$_2$ and HgCl$_2$ on CEM and nylon membranes have also been observed at above-ambient concentrations (Mao and Khalizov, 2021), suggesting that Hg^{II} compounds desorbed from nylon membranes could be different from atmospheric Hg^{II} compounds initially captured. <u>This may be true of any new Hg$^{II}_{(g)}$ sorptive surface, and should be considered during the validation of new materials.</u>

DCS circumvent the need for Hg^{II} preconcentration by converting Hg^{II} to Hg^0 using a thermolyzer and measuring total gaseous Hg. The Hg^{II} concentration can then be calculated by subtracting the Hg^0-only fraction of atmospheric air, obtained by scrubbing ambient sample of Hg^{II} with CEM, from the total gaseous Hg measurement. DCS have been successfully calibrated for Hg$^{II}_{(g)}$ measurement in the field, but do not provide Hg^{II} chemistry data (Lyman et al., 2020b).

~~Mass spectrometry (~~MS~~)~~ methods that can identify and quantify atmospheric Hg^{II} compounds could be an essential step towards describing Hg chemistry in the atmosphere, but unambiguous determination of the identity of Hg^{II} compounds via MS has not yet been achieved (cf. Deeds et al., 2015; Jones et al. 2016). Given the limitations of current Hg^{II} sorbents, new surfaces that can quantitatively capture Hg^{II} without compound-altering chemistry are needed to preconcentrate ambient samples to levels above MS detection limits. An ideal material for analysis of Hg^{II} compounds by MS will be inert to Hg^0, capture and retain all Hg^{II} compounds with high efficiency, not promote compound-altering reactions occurring on the material surface, and release atmospherically representative Hg compounds by thermal desorption for downstream analysis.

Characteristics of promising materials include: ion exchange with a porous or layered crystalline material (Manos and Kanatzidis, 2016); high surface area; and a high melting temperature that would facilitate thermal sample recovery and analysis by MS. Materials functionalized with sulfur, such as thiol, thiosemicarbazide, sulfone, and sulfonamide groups, show promise due to their high affinity for Hg^{II} (Yu et al., 2016). Capture efficiency is increased in base materials by functionalization with active groups that interact with Hg through chemisorption, resulting in the formation of a covalent bond between the Hg atom and material (Ali et al., 2018). However, strong bonding between the material and Hg^{II} may cause the identity of the Hg compound to be lost upon collection. As a result of strong bonding, such a material may not be suitable for subsequent analysis by MS methods. Materials that capture Hg by physisorption processes (electrostatic interactions) may be desirable if Hg compounds do not undergo chemistry on the sorbent surface, as has been observed for CEM and nylon membranes at high concentrations (Mao and Khalizov, 2021).

The objective of this work was to explore chitosan, α-Al$_2$O$_3$, γ-Al$_2$O$_3$, poly(1,4-phenylene sulfide), and perfluorosulfonic acid as candidate materials for preconcentration of atmospheric Hg^{II} that would be suitable for subsequent analysis by MS. A custom-built Hg^{II} permeation calibrator was used to load candidate materials with a known quantity of Hg^{II}, for comparison to CEM. Hg^{II} capture by these materials was also compared under field conditions. It was hypothesized that chitosan, α-Al$_2$O$_3$, and γ-Al$_2$O$_3$ would quantitatively sorb Hg^{II} under ambient conditions. Chitosan sorbs Hg^{II} through both chelation and electrostatic interactions in liquid matrices via amino and hydroxyl groups (Vieira and Beppu, 2006). α-Al$_2$O$_3$ and γ-Al$_2$O$_3$, alumina polymorphs, were potential materials of interest because they are polar compounds, but not acidic, and thus, may attract Hg$^{II}_{(g)}$ compounds without capturing Hg^0 (Zheng et al., 2019). Alumina polymorphs are stable at high temperatures (Baronskiy et al., 2022), making them ideal for re-use following thermal desorption. α-Al$_2$O$_3$ and γ-Al$_2$O$_3$ differ in thermal stability and specific surface area, and thus may perform differently in terms of capture efficiency and reusability.

2 Methods

2.1 Materials

CEM, polyethersulfone membranes that are proprietarily treated, were purchased from Pall Corporation (0.8 μm pore size; Mustang-S, P/N MSTGS3R) as sheets and cut to 47 mm diameter discs. PTFE membranes were purchased from Sartorius Stedim Biotech (0.2 μm pore size; P/N1180747). Chitosan (85% deacetylated; P/N J64143.18) and α-Al$_2$O$_3$ (< 1 μm, powder; P/N 0452572.22) were purchased from Thermo Scientific. γ-Al$_2$O$_3$ was obtained from Alpha Aesar as a 40 μm powder (P/N 043266.22). α-Al$_2$O$_3$ used in this study had a specific surface area of 2 - 4 m^2 g^{-1} and thermal stability of 1200 °C, while the γ-Al$_2$O$_3$ had a specific surface area of 100 m^2 g^{-1} and thermal stability up to 500 °C. Perfluorosulfonic acid membrane sheets (PFSA-M) were purchased from Sigma Aldrich (trade name Aquivion E98-05, PFSA equivalent weight 980 g mol^{-1} SO$_3$H, 50 μm film thickness; P/N 802697). Poly(1,4-phenylene sulfide) was also purchased from Sigma Aldrich (P/N 182354). Activated carbon was acquired from Aldrich Chemical Company (P/N 292591) as 4-14 mesh granules and crushed for use in experiments as a powder.

A set of glass tubes used to test PFSA-M were sent to SilcoTek for inert coating with deactivated silica (SilcoNert® 2000) to test if this improved Hg^{II} recovery. Based on the results of this test (discussed below), glass tubes without inert coating were used in laboratory and field tests. PTFE frits, which were 10-30 µm in pore size, 2.5 mm thickness, and cut to fit 6.35 mm diameter tubing, were acquired from Savillex (P/N: 730-0065), as were perfluoroalkoxyalkane filter packs used to house membranes (47 mm diameter, P/N 403-21-47-22-21-2). Optima™ HCl (A466-500), KBr (P205-500), NH$_2$OH·HCl (H330-500), and SnCl$_2$ (T142-500) were obtained from Fisher Scientific. KBrO$_3$ was purchased from Acros Organics (268392500). All reagents were ACS grade or higher and made with 18.2 MΩ-cm type 1 water. Ultra-high purity argon (Linde Gas and Equipment Inc.) was used in sorption tests

4

described in the Appendix. Gas-tight syringes were purchased from Hamilton Company (Reno, Nevada, USA). Flow rates in laboratory tests and field campaigns were controlled with critical flow orifices obtained from Teledyne API (941100).

145   Candidate materials that could potentially sorb $Hg^{II}_{(g)}$ without capturing Hg^0 were identified from the literature and preliminary work was performed to select promising materials for further experimentation. Of the five new materials tested, only three were considered for further investigation. Preliminary work indicated poor recovery of Hg^{2+} from two liquid-spiked poly(1,4-phenylene sulfide) samples when analyzed using a modified EPA Method 1631 digestion (United States Environmental Protection Agency, 2002). This suggested a matrix interference and this

150 material was not tested further. Investigation of PFSA-M was also discontinued after poor performance in $Hg^{II}_{(g)}$ laboratory tests (discussed below). Preliminary work with poly(1,4-phenylene sulfide) is detailed in the Appendix, with additional data for chitosan, α-Al$_2$O$_3$, and γ-Al$_2$O$_3$ (Appendix A and B). An alternative digestion method (the appendix to EPA Method 1631) for recovering Hg^{II} from CEM, chitosan, α-Al$_2$O$_3$, and γ-Al$_2$O$_3$ was attempted, and these data are also available in the Appendix (Appendix C).

Formatted: Not Superscript/ Subscript

155 **2.2 Laboratory loading of Hg^0 and $Hg^{II}_{(g)}$ onto candidate materials**

    Chitosan, α-Al$_2$O$_3$, γ-Al$_2$O$_3$, and PFSA-M were tested for quantitative Hg^0 and $Hg^{II}_{(g)}$ sorption in the laboratory. To test for sorption of Hg^0 to candidate materials, laboratory air was drawn at 1 L min^{-1} through traps containing test material. A syringe was used to inject 1.2 ng Hg^0 from a bell jar into the trap (n = 9). As a control, activated carbon was loaded by the same method. Traps containing 30 ± 5 mg of chitosan, α-Al$_2$O$_3$, γ-Al$_2$O$_3$, or

160 shredded PFSA-M were constructed with glass tubing containing a single PTFE frit. The glass tube (6.35 mm internal diameter) was slightly pinched at one end to prevent the frit and test material from being pulled through the trap during loading. Replicates (n = 9) of each material were exposed to laboratory air for three minutes, at the end of which the Hg^0 injection was made. Additional traps (n = 9 per material type) that were exposed to laboratory air, but not loaded with Hg^0, were used to blank-correct loaded samples. The mass of loaded Hg^0 was calculated based on the Dumarey

165 equation (Dumarey et al., 2010). Hg^0 recovered from candidate materials was compared both to the calculated mass loaded and to Hg^0 recovered from the method control. The syringe (Hg^0) tip was placed as close as possible to the materials during loading to minimize loss to the atmosphere or glass tubing.

    Hg^0 was recovered by combustion (EPA Method 7473) using a direct Hg analyzer (Nippon, MA-3000) (United States Environmental Protection Agency, 2007). This instrument was calibrated ($r^2 \geq 0.999$) with a primary

170 liquid Hg^{2+} standard (Inorganic Ventures, MSHG-1PPM). At the beginning of each analytical run, three aliquots of a secondary standard, National Institute of Standards and Technology Standard Reference Material 1547, were analyzed to demonstrate instrument performance. Two additional aliquots of 1547 were run every 10 samples or fewer to confirm ongoing instrument performance. A recovery within ± 10% if the certified value was considered acceptable for analysis. This instrument has a detection limit of 0.10 ng Hg^0.

175 ~~Sorption of $Hg^{II}_{(g)}$ to candidate materials was performed with the same procedure, using a custom built HgBr$_2$ calibrator (Allen et al., 2024; Gačnik et al., submitted).~~

5

~~The tip of the calibrator was inserted into the glass tubing to load candidate materials.~~ Sorption of $Hg^{II}_{(g)}$ to candidate materials was performed with the same procedure, using a custom-built $HgBr_2$ calibrator (Allen et al., 2024; Gačnik et al., 2024) that releases a constant stream of $Hg^{II}_{(g)}$ from a salt-based permeation source. The permeation rate is tightly controlled by maintaining constant temperature, pressure, and He flow over the permeation source. The permeation rate of the calibrator can be determined either gravimetrically or by measurement with CEM (Lyman et al., 2016; Gačnik et al., 2024). These methods have been demonstrated to be equivalent by Elgiar et al. (2024). The CEM method was used to calculate the permeation rate of the calibrator in this study. Briefly, permeation rates are calculated by exposing CEM to calibrator output, then digesting the CEM by EPA Method 1631. The recovered mass of Hg is then divided by the exposure time to provide a pg s^{-1} permeation rate (blank corrected). Although this calibrator can be used to calibrate $Hg^{II}_{(g)}$ measurements in other systems, it was used here to compare sorptive properties of candidate materials to CEM, by delivering consistent, measurable, quantities of $Hg^{II}_{(g)}$. Chitosan, α-Al_2O_3, γ-Al_2O_3, and nylon (n = 9 replicates each), PFSA-M (n = 6 replicates) were exposed to the calibrator output for the same duration, to ensure equal loading of $Hg^{II}_{(g)}$ for each replicate. Triplicate blanks of each material were also exposed to laboratory air for an equivalent period of time. Initial experiments loading CEM in this study measured a 1.76 ± 0.18 pg s^{-1} permeation rate (mean ± standard deviation, n = 9). The permeation rate of this calibrator was reported as 2.2 ± 0.2 pg s^{-1} in ~~concurrent experiments~~experiments performed concurrently, discussed elsewhere (Gačnik et al., 2024~~submitted~~). The difference in observed permeation rate between these two studies is of significance for the use of this system for calibrating Hg^{II} measurements and should be studied further before it is broadly employed by the research community. A possible explanation ~~may be explained by~~for the difference may be the positioning of the calibrator tip at a distance of 2 cm from the CEM during loading (Gačnik et al., 2024~~submitted~~) versus at the filter pack inlet (5.5 cm in this work), as $HgBr_2$ is more likely to come in contact with the filterpack when loaded at the inlet.~~.~~ Work by Allen et al. (2024) suggest less than 5% of atmospheric Hg^{II} is sorbed to the PTFE filterpacks after field deployment. ~~However, p~~

Permeation, as measured by CEM, dropped significantly to 0.42 ± 0.03 pg s^{-1} ~~in subsequent~~during experiment replication ~~experiments~~. It was suspected that the chamber containing the permeation tube over heated and shut off, cooling the $HgBr_2$ salt. Returning the heated chamber to 50 °C restored the measured permeation rate to 1.77 ± 0.06 (~~n = 9, data not shown~~data available in Appendix Table I1).

Due to the change in permeation rate across replicate experiments, results are reported as a % of $Hg^{II}_{(g)}$ recovered from CEM, rather than a % of the expected recovery based on the ~~validated~~ perm rate that was calculated as the mass of Hg^{II} recovered from CEM divided by exposure time (pg s^{-1}~~.~~). $Hg^{II}_{(g)}$ was quantified by following a modified version of EPA Method 1631. Briefly, BrCl solution (1.8% KBr and 1.2% $KBrO_3$ in 32-35% w/w Optima™ HCl) was added to candidate materials and membranes in 1% HCl at a ratio of 3 mL BrCl to 50 mL 1% HCl, and digested at room temperature overnight (see the SI of Dunham-Cheatham et al., 2023 for additional details). Samples were analyzed by cold vapor atomic fluorescence spectroscopy (Tekran 2600-IVS). The instrument was calibrated (r^2 ≥ 0.999) at the beginning and end of analysis. A check standard was analyzed every ten samples and the instrument was re-calibrated after a maximum of 30 samples were run. Data were considered acceptable if check standards were

6

recovered within ± 15% of the true value, as per EPA Method 1631. Blanks for each tested material were collected and analyzed with samples during each experiment, and were used to correct the analyzed value of samples. These blanks were exposed to laboratory air only (no $HgBr_2$) during laboratory $HgBr_2$ exposure tests, or were not exposed to air during field campaigns. Mean recovery on CEM blanks (exposed to laboratory air or not) was 0.03 ± 0.01 ng per membrane (± 1 standard deviation) across 28 replicates. Mean recovery of α-Al_2O_3, γ-Al_2O_3 and chitosan was 0.01 ± 0.02, 0.01 ± 0.01, and 0.02 ± 0.01 ng per target mass (30 mg), respectively (n = 27 for each material).

2.3 Field comparison of candidate materials and CEM

Candidate materials were deployed for three one-week sampling campaigns in the summer (late July through mid-September, 2023) at the University of Nevada, Reno College of Agriculture, Biotechnology & Natural Resources Agricultural Experiment Station Valley Road Greenhouse Complex (39.5375, −119.8047, 1370 masl). This sampling location is within 100 m of Interstate-80 and is impacted by vehicle emissions and long-range transport of pollutants (Gustin et al., 2021; Luippold et al., 2020a). Environmental conditions varied between campaigns, with weekly mean temperatures falling from 25.0 ± 0.5 °C in the first campaign to 22.0 ± 3.4 and 20.8 ± 0.6 °C in the last two campaigns. Relative humidity was 20 ± 4, 48 ± 16, and 35 ± 5 % for the first, second, and third campaigns, respectively. Temperature, relative humidity, solar radiation, and precipitation information was obtained from Western Regional Climate Center (https://raws.dri.edu/) measurement station located at the test site (39.53917, -119.806, 1370 masl), and is available in the Appendix (Table D1).

Traps, constructed as described for Hg^0 and $Hg^{II}_{(g)}$ sorption tests above, were deployed in inverted RMAS shields (Fig. E1). Three replicates of each material were deployed with a PTFE membrane upstream (to separate $Hg^{II}_{(g)}$ and $Hg^{II}_{(p)}$), and three replicate traps were deployed without an upstream PTFE membrane (providing a total Hg^{II} measurement). A CEM was deployed behind each candidate material to capture breakthrough $Hg^{II}_{(g)}$. Filter packs containing two consecutive CEM, both with and without an upstream PTFE membrane (n = 3 for each configuration), were co-deployed with candidate materials. Critical flow orifices controlled the flow across all collection materials at 1 L min^{-1}, and the flow rate through each trap or filter pack assembly was measured as standard flow at the beginning and end of each campaign using a volumetric air flow calibrator (BGI tetraCal). Measured masses of $Hg^{II}_{(g)}$ in each trap or filter pack were divided by the volume of air sampled, calculated as the average of flow rates measured at the beginning and end of deployment, in L min^{-1}, multiplied by the total sampling time in min, to calculate a $Hg^{II}_{(g)}$ concentration sampled in ambient air. All membranes and candidate materials were digested by the modified EPA Method 1631 procedure described above.

2.4 Statistical analysis

One-way ANOVA and Tukey's honestly significant difference tests ($\alpha \leq 0.05$), comparing the recovery of Hg^{II} between material types, were performed using R (R Core Team, 2023, version 2023.06.2+561). Means, standard deviations, and t-tests were calculated using Excel 2016.

3 Results and discussion

3.1 Laboratory tests for Hg^0 and Hg^{II}$_{(g)}$ sorption

      In this work, chitosan, α-Al$_2$O$_3$, and γ-Al$_2$O$_3$, were tested for sorption of Hg^0 and Hg^{II} in the laboratory and
the field. Additionally, preliminary Hg^{II}$_{(g)}$ sorption tests with poly (1,4-phenylene sulfide) and PFSA-M were
performed, but these materials were abandoned when a matrix interference was identified for (1,4-phenylene sulfide)
and PFSA-M demonstrated poor Hg^{II}$_{(g)}$ recovery. A summary of the materials tested and outcomes are available in
Table 1, and the details of preliminary work are available in ~~the~~ Appendix A and B. No quantifiable Hg^0 was recovered
from blanks or Hg^0-loaded chitosan, α-Al$_2$O$_3$, nor γ-Al$_2$O$_3$, except for one Hg^0-loaded γ-Al$_2$O$_3$ trap that had low
recovery (0.11 ng). Hg^0 recovery from activated carbon was 1.3 ± 0.4 ng (mean ± standard deviation), indicating
reasonably good agreement with the expected recovery of 1.1 ng, based on the Dumarey equation (Fig. F1).

Table 1. Outcomes of materials tested.

Material tested	Outcome of findings
Chitosan	Hg^{II}$_{(g)}$ was recovered quantitatively from chitosan under laboratory conditions, but less Hg^{II}$_{(g)}$ was recovered compared to CEM during field deployments. Ambient humidity may have interfered with Hg^{II}$_{(g)}$ capture by chitosan.
α-Al$_2$O$_3$	Less Hg^{II}$_{(g)}$ was recovered from α-Al$_2$O$_3$ compared to CEM under both laboratory and field conditions. EPA Method 1631 may be insufficient to quantitatively recover Hg^{II}$_{(g)}$ from this matrix.
γ-Al$_2$O$_3$	Less Hg^{II}$_{(g)}$ was recovered from γ-Al$_2$O$_3$ compared to CEM under both laboratory and field conditions. EPA Method 1631 may be insufficient to quantitatively recover Hg^{II}$_{(g)}$ from this matrix.
Poly(1,4-phenylene sulfide)	Poor recovery of liquid Hg^{II} from spiked poly(1,4-phenylene sulfide) indicated a matrix interference when digested by EPA Method 1631.
Polyflourosulfonic acid membrane (PFSA-M)	Poor recovery of Hg^{II}$_{(g)}$ from this material was observed compared to CEM under laboratory conditions.

      Chitosan traps recovered 99 ± 36% of the loaded Hg^{II}$_{(g)}$ compared to the CEM, while α-Al$_2$O$_3$, γ-Al$_2$O$_3$,
nylon, and PFSA-M recovered less (86 ± 15%, 69 ± 21%, 81 ± 7%, and 26 ± 7%, respectively) (Fig. 1). Due to the
smaller quantities of Hg^{II}$_{(g)}$ loaded following the drop in permeation, small variation in mass Hg^{II}$_{(g)}$ recovered
resulted in a larger % variation. Variation in mass Hg^{II}$_{(g)}$ recovered from both the candidate material and CEM also
contributed. Given the low recovery of Hg^{II}$_{(g)}$ from PFSA-M, it was not tested further. As breakthrough was not
quantified for this material, it is unclear if the low recovery is due to low capture efficiency of the material itself, or
if the geometry of the trap (shredded membrane packed into glass tubing) permitted greater breakthrough. If this
membrane material could be made porous, or functionalized onto a porous substrate, it may demonstrate increased
capture of Hg^{II}$_{(g)}$ due to the presence of sulfonic acid functional groups. A comparison of Hg^{II}$_{(g)}$ recoveries was made
between PFSA-M membranes that were loaded with Hg^{II}$_{(g)}$ in glass tubing coated with deactivated fused silica, or in
uncoated glass tubing. Although it was hypothesized that the coating would reduce Hg^{II}$_{(g)}$ sorption to the glass

8

270 tubing (Jones et al., 2016), $Hg^{II}_{(g)}$ recovery was not statistically different between PFSA-M samples loaded in
deactivated fused silica coated or uncoated tubes ($p > 0.05$; Fig. G1). $Hg^{II}_{(g)}$ recovered on CEM downstream of other
candidate materials provided a measurement of $Hg^{II}_{(g)}$ breakthrough, calculated as a % of the sum of $Hg^{II}_{(g)}$
recovered from the candidate material plus the CEM ($n = 6$ replicates for chitosan, α-Al_2O_3, γ-Al_2O_3, and nylon). An
average of $\leq 5\%$ $Hg^{II}_{(g)}$ was recovered downstream of candidate materials, and no quantifiable $Hg^{II}_{(g)}$ was recovered
275 on the second-in-line CEM behind a CEM.
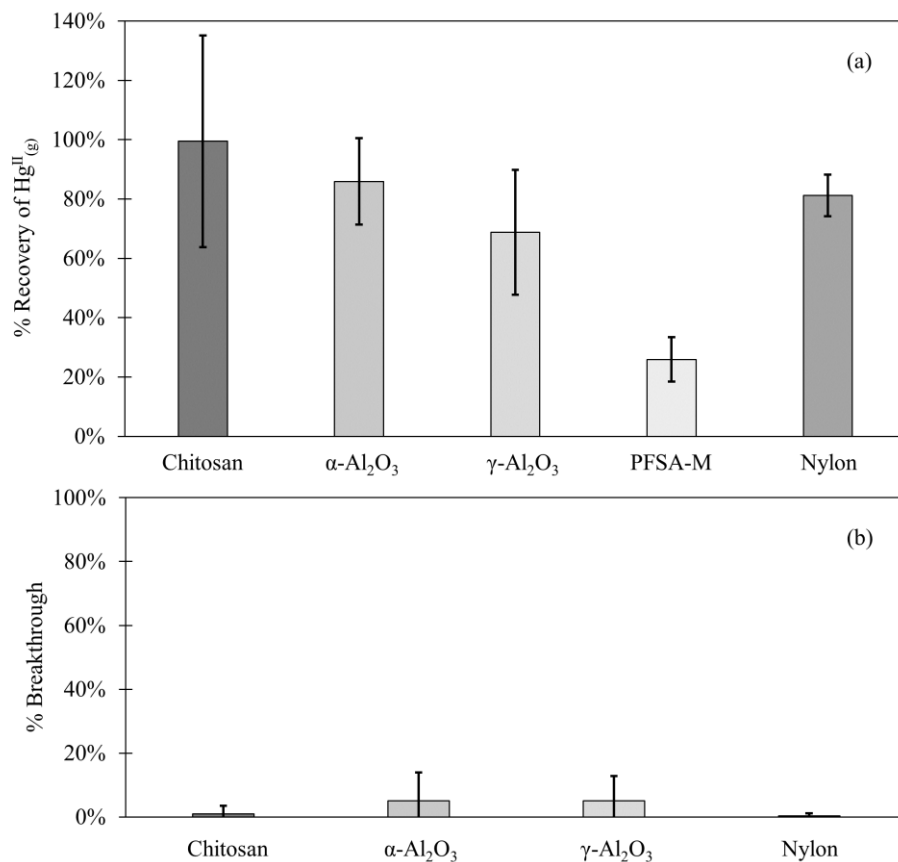
Figure 1. (a) $Hg^{II}_{(g)}$ recovered from candidate materials ($n = 9$ each for chitosan, α-Al_2O_3, γ-Al_2O_3, and nylon, and n
$= 6$ for PFSA-M) loaded with $HgBr_2$ in laboratory air, as a percentage of $HgBr_2$ recovered on CEM. (b) $Hg^{II}_{(g)}$
breakthrough from candidate materials ($n = 6$ each) as a % of $HgBr_2$ collected on CEM. Error bars represent one
280 standard deviation from the mean.

9

The relatively low recovery of $Hg^{II}_{(g)}$ from α-Al_2O_3 and γ-Al_2O_3, as well as the minimal breakthrough, indicated that $Hg^{II}_{(g)}$ was either lost during loading, possibly to the glass tubing, or it was not recovered from the material matrix by BrCl digestion. Al_2O_3 has been previously used to capture and thermally reduce Hg^{II} to Hg^0 with high efficiency in an inert atmosphere (Gačnik et al., 2022), suggesting the EPA Method 1631 digestion is not sufficient to recover Hg^{II} sample from this matrix. Chitosan, an organic compound, is more easily decomposed, and thus, sorbed Hg is made more available for analysis by acid digestion compared to oxide crystals like α-Al_2O_3 and γ-Al_2O_3. This may explain why a higher % recovery was observed from chitosan compared to α-Al_2O_3 and γ-Al_2O_3, and highlights the need to consider alternative digestion methods, or possibly thermal desorption, and utilize matrix-matched certified reference materials when considering new surfaces for quantitative $Hg^{II}_{(g)}$ capture.

Digestions with HF and HNO_3 have been used to recover metals from refractory silicates and oxides (Zimmermann et al., 2020), and EPA Method 3052 (United States Environmental Protection Agency, 1996) is an established method for Hg. It aims to completely decompose and dissolve the sample by microwave digestion with HF and HNO_3, but also offers alternative matrix-specific reagent mixtures with HCl and H_2O_2. This method notes that it may not be suitable for some oxides, including Al_2O_3 and TiO_2, among others, and that target analytes (including Hg) can be sequestered by undecomposed sample, leading to low recovery. Re-adsorption of Hg by residual sample matrix during digestion is also noted for activated carbon matrices in the appendix to EPA Method 1631 and could explain low $Hg^{II}_{(g)}$ recovery from the α-Al_2O_3 and γ-Al_2O_3 in this study. Microwave digestion of $Hg^{II}_{(g)}$ loaded carbon and γ-Al_2O_3 with HBF_4 was attempted as a safer alternative to digestion with HF (Zimmermann et al., 2020), but high background Hg in analytical-grade reagents made data inconclusive. Direct Hg analyzers conveniently overcome matrix interferences by combusting the sample, but atmospheric samples will need to be preconcentrated over 2-week campaigns to collect enough Hg to exceed analytical detection limits, limiting the utility of this method for analyzing Hg^{II} trends over short timescales.

3.2 Hg^{II} recovery from candidate materials in the field

Candidate materials were deployed with or without a PTFE membrane upstream, and with a CEM downstream. Of the total Hg^{II} recovered from PTFE + Al_2O_3 traps, 66% was recovered from the PTFE portion of α-Al_2O_3 traps and 55% of Hg^{II} was recovered from the PTFE on γ-Al_2O_3 traps, indicating that half or more of the Hg^{II} recovered was particulate-bound or $Hg^{II}_{(g)}$ sorbed to particles (see below). More $Hg^{II}_{(g)}$ was captured on chitosan behind PTFE compared to the equivalent α-Al_2O_3 and γ-Al_2O_3 traps (an average across all three campaigns of 7 ± 3 pg m^{-3} α-Al_2O_3 vs 28 ± 43 pg m^{-3} γ-Al_2O_3 and 46 ± 36 pg m^{-3} chitosan), but not as much as compared to CEM (91 ± 45 pg m^{-3}). This agrees with the laboratory tests that show poor $Hg^{II}_{(g)}$ recovery from α-Al_2O_3 and γ-Al_2O_3 and relatively greater $Hg^{II}_{(g)}$ recovery from chitosan. Total Hg^{II} recovery from the entire trap assembly (PTFE membrane (if present) + candidate material or first-in-line CEM + breakthrough CEM) was not statistically different between chitosan and CEM traps during any campaign. Recovery was statistically lower for α-Al_2O_3 and γ-Al_2O_3 in the first and third campaigns, and higher for α-Al_2O_3 during the second campaign (Fig. H1(a)). Field measurements included a downstream CEM that captured Hg^{II} not sorbed by candidate materials (i.e. "breakthrough") Hg^{II}, if present. These

data also suggest that either BrCl digestion was not sufficient to recover Hg^{II} from Al_2O_3 matrices or reduction was occurring on the material surface during the week-long sampling period and Hg^{II} was lost as Hg^0.

Recent work by Allen et al. (2024) demonstrated that $Hg^{II}_{(g)}$ can be sorbed by particulates on PTFE filters, suggesting that $Hg^{II}_{(p)}$ measurements are biased high with additional $Hg^{II}_{(g)}$ sorbed. For this reason, Hg^{II} recovered on PTFE filters was added to $Hg^{II}_{(g)}$ recovered from downstream candidate materials to yield a total Hg^{II} measurement, and these data were combined with Hg^{II} measurements from candidate materials without upstream PTFE. The sum of $Hg^{II}_{(p)} + Hg^{II}_{(g)}$ recovered from PTFE + CEM, respectively, has been well correlated with Hg^{II} measurements on CEM in previous work (Gustin et al., 2019; Gustin et al., 2023). CEM (n = 6, three of which included Hg^{II} recovery from PTFE + CEM) recovered the highest mass Hg^{II} m^{-3} air sampled of all materials tested (Fig. 2(a)). More than 20% of the Hg^{II} recovered from the entire trap (PTFE membrane, candidate material, and breakthrough CEM) was recovered downstream of candidate materials (Fig. 2(b)), indicating that chitosan, α-Al_2O_3, and γ-Al_2O_3 did not quantitatively measure $Hg^{II}_{(g)}$ under field conditions. There was a decrease in the Hg^{II} measured by all materials in the second and third campaigns that coincided with periods of rain and increased humidity, which is consistent with observations of Hg^{II} washout during rain events (Kaulfus et al., 2017). Of the candidate materials, chitosan performed the best during the first campaign, recovering a similar quantity of Hg^{II} as CEM, but decreased in relative recovery during the second and third campaigns. Chitosan is highly hygroscopic (Szymańska and Winnicka, 2015), and the amino functional groups on chitosan are easily protonated at pH < 6, thus it is possible the increased humidity led to a decrease in $Hg^{II}_{(g)}$ sorption capacity due to electrostatic repulsion between protonated amino groups and $Hg^{II}_{(g)}$ (Vieira and Beppu, 2006).
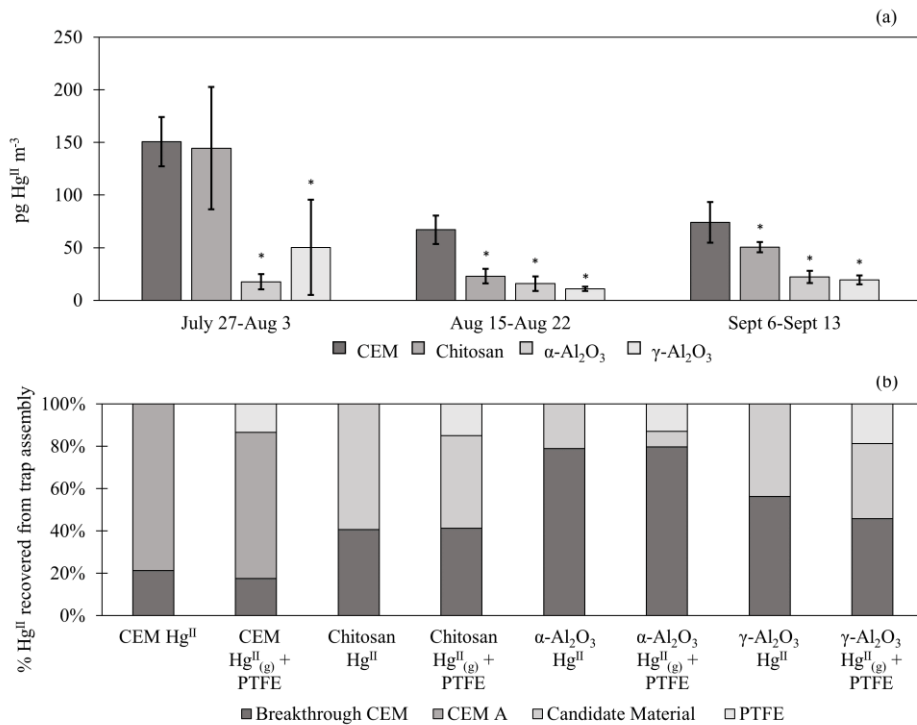
Figure 2. (a) Hg^{II} recovery from PTFE + candidate materials deployed in the field for three one-week campaigns. Hg^{II} recovery from traps with first-in-line PTFE membranes ($Hg^{II}_{(g)}$ +$Hg^{II}_{(p)}$) were combined with traps without PTFE (Hg^{II}) for statistical analysis (n = 6 per campaign). Data do not include $Hg^{II}_{(g)}$ recovered on breakthrough CEM. Error bars are one standard deviation from the mean. Asterisks (*) indicate a statistically different recovery of $Hg^{II}_{(g)}$ on candidate materials compared to CEM (ANOVA, $\alpha \leq 0.05$). (b) The % of Hg^{II} recovered from each portion of the trap assembly, including from the PTFE, candidate material, first-in-line CEM (CEM A), and/or breakthrough CEM. Hg^{II} traps with no upstream PTFE are shown separately from $Hg^{II}_{(g)}$ + PTFE traps.

4 Conclusions

CEM outperformed chitosan, α-Al$_2$O$_3$, and γ-Al$_2$O$_3$ for $Hg^{II}_{(g)}$ measurement in the laboratory and the field, indicating they do not quantitatively capture Hg^{II}. Candidate materials did not collect Hg^0. Low recoveries of $Hg^{II}_{(g)}$ from α-Al$_2$O$_3$ and γ-Al$_2$O$_3$ may be due to insufficient digestion methods, demonstrating a need for using matrix-

12

specific methods with certified reference materials when testing alternative materials in the future. Promising materials should be tested for: sorption of $Hg^{II}_{(g)}$ and Hg^0, capture efficiency for a broad range of representative Hg compounds (Dunham-Cheatham et al., 2020); the potential for chemical transformation on the material surface; and potential reactions between the Hg sample and other atmospheric constituents, including interferences with humidity (Huang and Gustin, 2015) and ozone (McClure et al., 2014); and for performance under both laboratory and field conditions.

Appendices

Appendix A: Preliminary assessment of gaseous elemental mercury sorption in an argon atmosphere to poly(1,4-phenylene sulfide), chitosan, perfluorosulfonic acid, and α-Al₂O₃

Cold vapor atomic fluorescence spectroscopy was used to characterize the loss of Hg in an argon (Ar) carrier gas following injection of gaseous elemental mercury (Hg^0) through a trap containing poly(1,4-phenylene sulfide) (PPS), chitosan, or a shredded perfluorosulfonic acid membrane (PFSA-M). The testing apparatus (Fig. A1) consisted of: an Ar cylinder that provided carrier gas and pressure to the sample line; a PTFE sample line into which a trap containing a test material could be inserted with an upstream Hg^0 injection port; a thermolyzer (> 650 °C) to convert gaseous oxidized mercury ($Hg^{II}_{(g)}$) to Hg^0; a gold cartridge to collect Hg^0 for analysis; and a Tekran 2500 to measure Hg^0. Materials were loaded with a gas-tight syringe by injecting Hg^0 from a temperature-stabilized source through the injection port upstream of a trap containing a sorbent material. The quantity of Hg^0 loaded was calculated based on the Dumarey equation (Dumarey et al., 2010). Sorbent traps containing 29.4 mg PPS, 29.4 mg chitosan, or a half of a 47 mm diameter PFSA-M (one replicate each) were constructed as described in the main text with 6.35 mm internal diameter uncoated glass tubing and quartz wool plugs.

To test for sorption of Hg^0 to PPS, chitosan, and PFSA-M, the peak area of 0.4 ng Hg^0 detected downstream of traps containing material was compared to a baseline peak area of 0.4 ng Hg^0 injected through a glass trap without sorbent material. Peaks observed following an injection indicated no or partial sorption of Hg^0 to the candidate material. A student's t-test ($\alpha = 0.05$) was used to assess if peak area of Hg^0 detected downstream of the candidate material (n = 5 injections of 0.4 ng Hg^0 each, relative standard deviation (RSD) < 10% for PPS) was statistically different from Hg^0 peak area detected downstream of the empty trap (n = 5 injections, RSD = 7%). The absence of a peak following an injection indicated complete sorption of Hg^0 to the trap, while significantly lower peak areas indicated partial sorption, and peak areas equivalent to peaks detected downstream of an empty trap indicated no Hg^0 sorption to the candidate material. PPS and chitosan did not sorb any Hg^0. More Hg^0 was recovered downstream of PFSA-M membranes compared to empty glass traps (RSD of injections < 5 %, p < 0.01). The reason for this was unclear and this test was repeated a second time with the same outcome (a total of 20 injections through each empty and PFSA-M trap over two days). It was concluded that PFSA-M did not sorb Hg^0.

A trap containing 14 mg α-Al₂O₃ was tested using a similar procedure with a few minor differences. The glass tubing was pinched at one end and contained PTFE frits, rather than quartz wool plugs, to prevent material movement, and the Tekran 2500 was calibrated with Hg^0 using the bell jar method ($r^2 > 0.998$) to quantify sorption by

13

α-Al$_2$O$_3$. The quantity of Hg^0 injected was also increased from 0.4 to 1.1 ng Hg so analysis was performed on a Hg mass in the middle of the calibration range. α-Al$_2$O$_3$ sorbed 40% of the injected Hg^0, demonstrating that significant sorption of Hg^0 is possible in an Ar atmosphere.
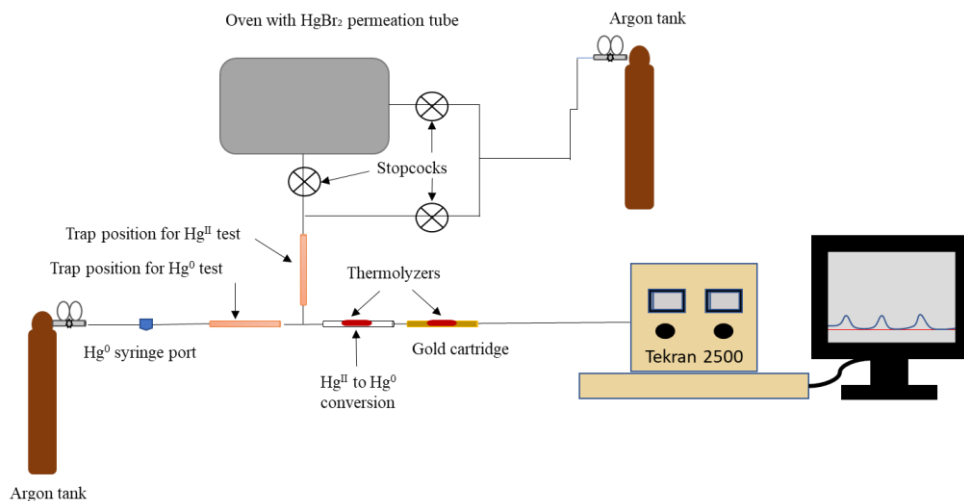
Fig. A1: Experimental setup for Hg^0 and Hg^{II}$_{(g)}$ sorption to candidate materials in an argon atmosphere. During Hg^0 sorption testing, the line containing the Hg^{II}$_{(g)}$ permeation tube was disconnected. Lines leading into the permeation source and to the Tekran 2500 were heated to a nominal 83 °C with heat tape and insulated with aluminum foil to encourage Hg^{II}$_{(g)}$ movement through the system and reduce photo-effects. Components in figure are not to scale.

Appendix B: Preliminary assessment of Hg^{II}$_{(g)}$ sorption to PFSA-M and PPS in an argon atmosphere

To test Hg^{II}$_{(g)}$ sorption to candidate materials, the experimental apparatus included a heated (nominally 90 °C) impinger containing a HgBr$_2$ permeation tube (Fig. A1) that could provide controlled injections of Hg^{II}$_{(g)}$ through a candidate material trap (35.6 mg PPS or a half of a 47 mm diameter PFSA-M membrane). For Hg^{II} tests, the sample line was also kept warm with heat tape (~83 °C) and insulated with aluminum foil. The same injection procedure as described above was used to determine Hg^{II}$_{(g)}$ sorption to PPS and PFSA-M, although the empty trap contained PTFE plugs rather than quartz wool. To confirm Hg^{II}$_{(g)}$ source stability over time, peak area was observed through an empty trap before and after Hg^{II}$_{(g)}$ injections, and a t-test was used to check that peak area from injections did not differ from the beginning of the test to the end of the test. Beginning and end injections were not statistically different in peak area.

Statistically different peak areas ($p < 0.05$) were observed between an empty glass trap and both PFSA-M and PPS, indicating these materials sorbed $Hg^{II}_{(g)}$ ($n = 5$, RSD $\leq 10\%$ for injections through an empty trap; $n = 5$, RSD $< 10\%$ for PFSA-M; and $n = 5$, RSD $= 14\%$ for injections through the PPS trap).

Appendix C: Appendix to EPA Method 1631

An alternative digestion method was attempted to improve recovery of $Hg^{II}_{(g)}$ from α-Al_2O_3 and γ-Al_2O_3. The appendix to EPA Method 1631 is a similar digestion procedure to Method 1631, but with an additional leaching step using aqua regia (3:1 HCl:HNO$_3$) before digestion with BrCl. A $Hg^{II}_{(g)}$ calibrator (described in the main text) was used to load materials with a known mass of $Hg^{II}_{(g)}$, in lieu of an appropriate certified reference material. An expected 0.25 ng $Hg^{II}_{(g)}$ was loaded onto each material (30 ± 5 mg chitosan, α-Al_2O_3, or γ-Al_2O_3; $n = 3$ traps each), which was then digested by the appendix to EPA Method 1631 and analyzed by cold vapor atomic fluorescence. Activated carbon (30 ± 5 mg) was used downstream of chitosan, α-Al_2O_3, and γ-Al_2O_3 to measure $Hg^{II}_{(g)}$ not captured by the candidate material. A second-in-line cation exchange membrane (CEM) captured breakthrough from a first-in-line CEM. All measurements were blank corrected with the appropriate material. Results were highly variable for α-Al_2O_3 (0.13 ± 0.12 ng $Hg^{II}_{(g)}$ recovered on α-Al_2O_3, and 0.17 ± 0.15 on breakthrough carbon), and no $Hg^{II}_{(g)}$ was recovered from γ-Al_2O_3 with little $Hg^{II}_{(g)}$ recovered from downstream carbon (0.03 ± 0.06 ng $Hg^{II}_{(g)}$). CEM reasonably recovered the expected loaded mass (0.23 ± 0.06 ng $Hg^{II}_{(g)}$), with no quantifiable breakthrough (Fig. C1). The expected 0.25 ng of $Hg^{II}_{(g)}$ was reasonably recovered from traps containing chitosan and breakthrough activated carbon (0.13 ± 0.06 ng recovered on chitosan, 0.1 ng recovered on downstream activated carbon) indicating that the appendix method worked to recover the mass balance from CEM, chitosan, and carbon matrices. The lack of $Hg^{II}_{(g)}$ recovery from α-Al_2O_3, γ-Al_2O_3 and downstream carbon suggest that α-Al_2O_3 and γ-Al_2O_3 may be sorbing Hg^{II} but this digestion method is insufficient to quantify it. The appendix to EPA Method 1635 was chosen as a digestion procedure because it is intended for recalcitrant matrices, including coal; however, aqua regia has a matrix-dependent leaching efficiency (Zimmermann et al., 2020). A certified reference material matrix matched to Al_2O_3 may conclusively demonstrate this.
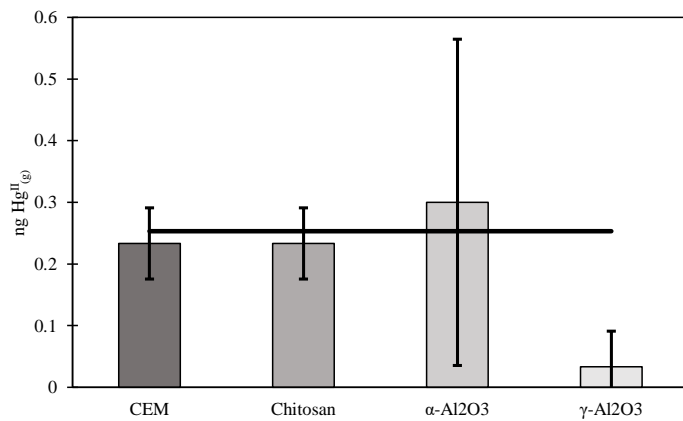
Fig. C1: $Hg^{II}_{(g)}$ (ng) recovered by the appendix to EPA Method 1631 on chitosan, α-Al_2O_3, and γ-Al_2O_3 compared to an equivalent mass of $Hg^{II}_{(g)}$ loaded on CEM. Masses include $Hg^{II}_{(g)}$ measured on downstream activated carbon. Error
430 bars represent one standard deviation from the mean.

Table D1: Environmental conditions during Reactive Mercury Active Systemampler (RMAS) campaigns. These data were downloaded as shown from the Western Regional Climate Center (https://raws.dri.edu/). The measurement station was located at the test site (39.53917, -119.806, 1370 masl). Means and standard deviations (highlighted in green) were calculated by the authors from the presented data.

| Date	Total Solar Radiation (ly)	Mean Air Temperature (°C)	Max. Mean Air Temperature (°C)	Min. Mean Air Temperature (°C)	Mean Relative Humidity (%)	Max. Mean Relative Humidity (%)	Min. Mean Relative Humidity (%)	Total Precipitation (cm)
Campaign 1								
7/27/23	759.1	24.9	33.0	14.4	28	56	15	0.0
7/28/23	761.8	25.6	33.2	13.7	23	50	13	0.0
7/29/23	554.3	25.1	33.4	17.4	24	46	13	0.0
7/30/23	766.2	25.6	33.7	13.7	23	50	11	0.0
7/31/23	710.7	25.4	34.2	14.2	23	50	12	0.0
8/1/23	681.4	24.7	35.1	15.3	28	49	13	0.0
8/2/23	612.0	24.8	34.4	15.7	33	59	15	0.0
8/3/23	713.6	24.3	32.8	14.9	32	64	17	0.0
Weekly mean	694.9	25.0	33.7	14.9	27	53	14	0.0
Standard deviation	76.6	0.5	0.8	1.3	4	6	2	0.0
Campaign 2								
8/15/23	545.6	23.7	34.4	13.1	50	96	18	0.0
8/16/23	598.7	25.5	36.7	14.9	41	72	16	0.0
8/17/23	527.9	25.7	33.7	19.3	44	77	21	0.0
8/18/23	547.7	23.7	33.2	14.4	42	76	18	0.0
8/19/23	528.4	23.3	32.9	15.2	41	71	15	0.0
8/20/23	215.7	18.0	21.6	15.0	76	98	53	0.5
8/21/23	317.9	17.8	23.6	13.7	73	98	44	0.3
8/22/23	414.5	18.1	25.5	12.6	66	96	34	0.1
Weekly mean	462.1	22.0	30.2	14.8	54	86	27	0.1
Standard deviation	133.9	3.4	5.7	2.1	15	12	15	0.2
Campaign 3								

17

9/6/23	587.7	20.4	28.8	11.8	53	91	24	0.0
9/7/23	595.8	20.1	30.3	9.9	47	87	15	0.0
9/8/23	597.3	20.0	30.4	8.3	42	81	12	0.0
9/9/23	570.2	21.1	31.3	10.5	45	79	17	0.0
9/10/23	580.9	21.4	31.0	11.0	44	82	20	0.0
9/11/23	565.2	21.7	31.7	11.2	40	76	18	0.0
9/12/23	523.0	21.1	30.5	10.8	39	68	19	0.0
9/13/23	551.8	20.6	28.9	11.5	40	70	21	0.0
Weekly mean	571.5	20.8	30.4	10.6	44	79	18	0.0
Standard deviation	25.0	0.6	1.1	1.1	5	8	4	0.0

435

Formatted: Centered

Formatted: Centered

Formatted: Centered

Formatted: Centered

Formatted: Centered

Formatted: Centered

Formatted: Centered

Formatted: Centered

**Formatted:** Centered

Formatted: Centered
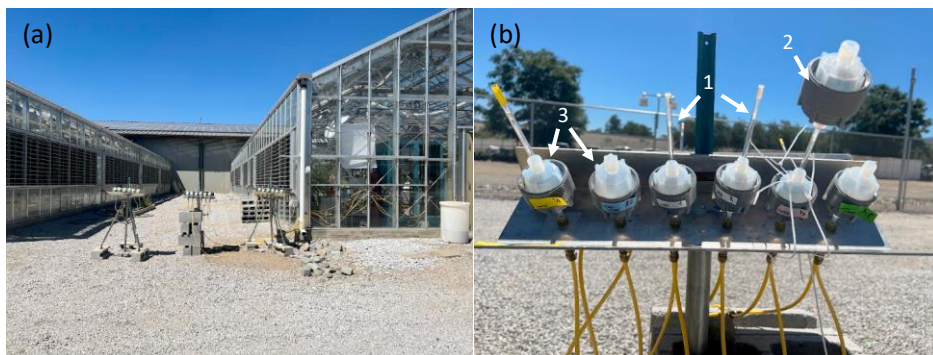
Fig. E1: (a) Field campaign of candidate materials and CEM in inverted RMAS shields. (b) A close-up of an inverted RMAS shield holding: (1) glass traps with candidate materials; (2) PTFE membranes; and (3) breakthrough CEM.

440
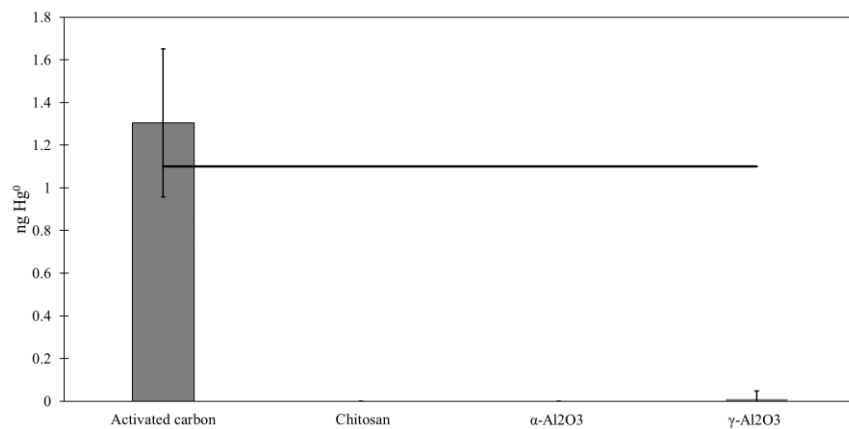
Fig. F1: Recovery of Hg^0 from activated carbon and candidate materials loaded in ambient air by syringe injection. The blacnk line indicates the calculated mass (1.1 ng Hg^0) loaded based on the Dumarey equation.

445
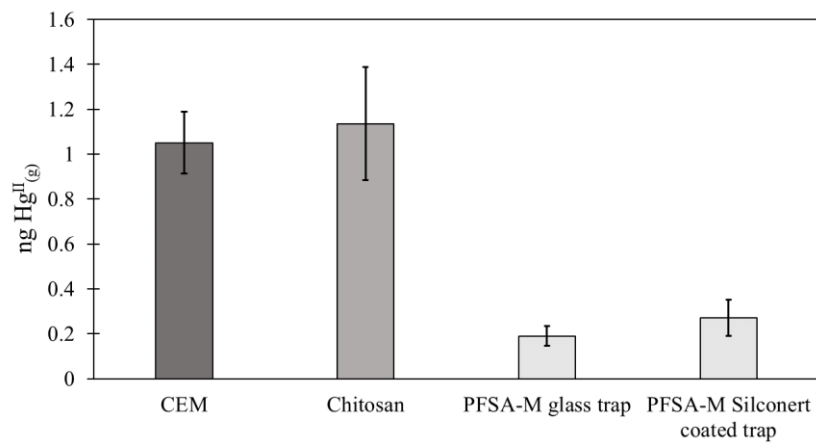
Fig. G1: $Hg^{II}_{(g)}$ recovery from PFSA-M using deactivated fused silica coated and uncoated glass tubes, compared to recovery from CEM and chitosan. The recovery of $Hg^{II}_{(g)}$ from PFSA-M was not statistically different between coated and uncoated glass traps ($p > 0.05$, two-sample t-test).
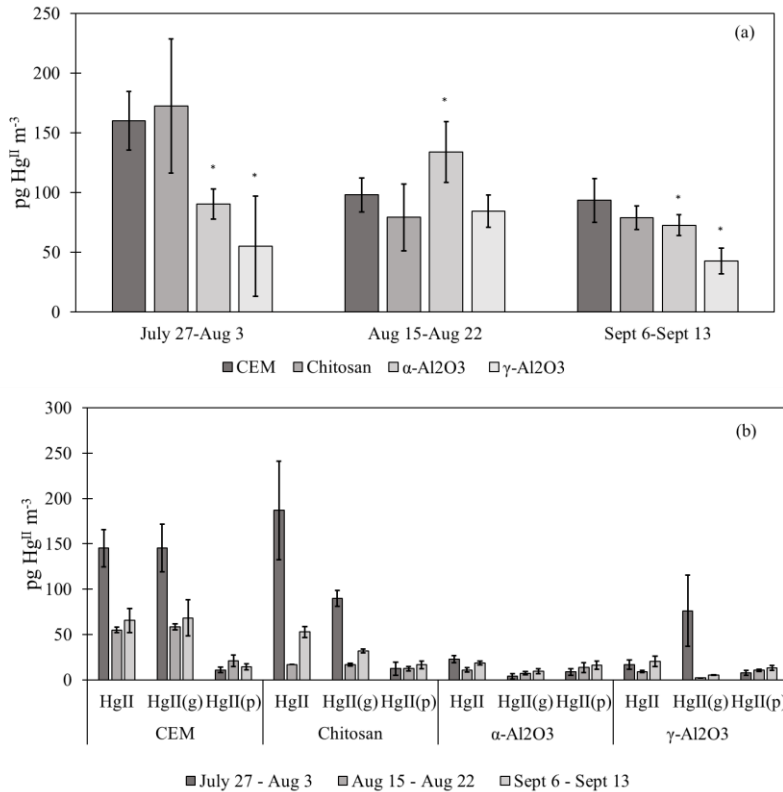
450

Fig. H1: (a) Total Hg^{II} recovery from entire trap assembly (PTFE membrane (if present) + candidate material or first-in-line CEM + breakthrough CEM). Data combine traps with and without upstream PTFE membranes for each material type (n = 6). Error bars represent one standard deviation from the mean. Asterisks (*) indicate a statistically different recovery of Hg^{II} on candidate materials compared to CEM (ANOVA, $\alpha \leq 0.05$). (b) Total Hg^{II} recovered from candidate materials or first-in-line CEM without upstream PTFE membranes (Hg^{II}; n = 3) shown adjacent to downstream candidate materials or CEM in traps with upstream PTFE (Hg$^{II}_{(g)}$; n = 3) and Hg^{II} recovered from PTFE membranes (Hg$^{II}_{(p)}$). In theory, Hg$^{II}_{(g)}$ + Hg$^{II}_{(p)}$ = Hg^{II}.

460   **Table I1:** Calibrator permeation rates as measured by CEM

Date	Average (pg s^{-1} ± 1σ)	Number of replicates

21

4/15/2023	1.71 ± 0.35	3
4/21/2023	1.79 ± 0.08	3
7/21/2023	1.78 ± 0.06	3
11/4/2023	0.27 ± 0.09*	3
11/18/2023	0.43 ± 0.08*	3
1/18/2024	1.82 ± 0.14	3
1/25/2024	1.83 ± 0.07	3
1/29/2024	1.71 ± 0.05	3
2/15/2024	1.76 ± 0.19	3

* $Hg^{II}_{(g)}$ source was not heated during loading.

465 **Table J1:** pg m^{-3} recoveries of Hg^{II} from traps following field deployment. Columns labeled Hg^{II} and Hg^{II} breakthrough belong to traps deployed without PTFE membranes. Recoveries (pg m^{-3}) of Hg^{II} from PTFE are indicated as $Hg^{II}_{(g)}$, recoveries from CEM or candidate material downstream of PTFE are indicated by $Hg^{II}_{(g)}$, and breakthrough from traps with PTFE membranes are indicated by $Hg^{II}_{(g+p)}$ breakthrough.

Material	Hg^{II}	Hg^{II} breakthrough	$Hg^{II}_{(p)}$	$Hg^{II}_{(g)}$	$Hg^{II}_{(p+g)}$ breakthrough
July 27 - Aug 3					
CEM	145 ± 20	0 ± 0	11 ± 3	145 ± 27	0 ± 0
Chitosan	187 ± 54	28 ± 15	12 ± 7	90 ± 9	27 ± 10
α-Al$_2$O$_3$	23 ± 4	62 ± 12	9 ± 4	4 ± 3	83 ± 15
γ-Al$_2$O$_3$	17 ± 5	9 ± 16	8 ± 3	76 ± 39	0 ± 30
Aug 15 - Aug 22					
CEM	55 ± 3	0 ± 0	21 ± 6	58 ± 3	0 ± 0
Chitosan	17 ± 0	42 ± 13	12 ± 2	17 ± 2	70 ± 27
α-Al$_2$O$_3$	11 ± 2	115 ± 14	14 ± 5	7 ± 2	121 ± 27
γ-Al$_2$O$_3$	9 ± 1	71 ± 17	11 ± 1	2 ± 0	76 ± 12
Sept 6 - Sept 13					
CEM	65 ± 13	0 ± 0	14 ± 3	68 ± 20	0 ± 0
Chitosan	53 ± 6	33 ± 5	17 ± 4	32 ± 2	24 ± 1
α-Al$_2$O$_3$	19 ± 2	49 ± 5	16 ± 4	10 ± 3	52 ± 3
γ-Al$_2$O$_3$	20 ± 6	27 ± 8	13 ± 3	5 ± 0	20 ± 4

Data/code availability

470 All data are included in the article and appendix.

Author contributions

LL suggested materials, designed and executed the experiments, performed data analysis and interpretation, and prepared the manuscript. SMDC suggested materials, supervised the experiments and data analysis, and edited the
475 manuscript. SNL built and consulted on the use of the $HgBr_2$ calibrator, consulted on other experiments, and edited the manuscript. MSG conceived the project and acquired funding, suggested materials, supervised experiments and edited the manuscript.

Competing interests

480 None of the authors have competing interests.

490 **References**

Ali, Z., Ahmad, R., Khan, A., and Adalata, B.: Complexation of Hg(II) ions with a functionalized adsorbent: A thermodynamic and kinetic approach, Prog. Nucl. Energ., 105, 146–152, https://doi.org/10.1016/j.pnucene.2018.01.004, 2018.

Allen, N., Gačnik, J., Dunham-Cheatham, S. M., and Gustin, M. S.: Interaction of reactive mercury with surfaces and
495 implications for atmospheric mercury speciation measurements, Atmos. Environ., 318, 120240, https://doi.org/10.1016/j.atmosenv.2023.120240, 2024.

Ariya, P.A., Amyot, M., Dastoor, A., Deeds, D., Feinberg, A., Kos, G., Poulain, A., Ryjkov, A., Semeniuk, K., Subir, M. and Toyota, K.: Mercury physicochemical and biogeochemical transformation in the atmosphere and at atmospheric interfaces: A review and future directions, Chem. Rev., 115, 3760-3802,
500 https://doi.org/10.1021/cr500667e, 2015.

Baronskiy, M. G., Tsybulya, S. V., Kostyukov, A. I., Zhuzhgov, A. V., and Snytnikov, V. N.: Structural properties investigation of different alumina polymorphs (η-, γ-, χ-, θ-, α-Al2O3) using Cr3+ as a luminescent probe, J. Lumin., 242, 118554, https://doi.org/10.1016/j.jlumin.2021.118554, 2022.

Deeds, D. A., Ghoshdastidar, A., Raofie, F., Guérette, E. A., Tessier, A., & Ariya, P. A.: Development of a particle-trap preconcentration-soft ionization mass spectrometric technique for the quantification of mercury halides in air, Anal. Chem., 87, 5109-5116, https://doi.org/10.1021/ac504545w, 2015.

Driscoll, C. T., Mason, R. P., Chan, H. M., Jacob, D. J., & Pirrone, N.: Mercury as a global pollutant: sources, pathways, and effects, Environ. Sci. Technol., 47, 4967-4983, https://doi.org/10.1021/es305071v, 2013.

Dumarey, R., Brown, R. J. C., Corns, W. T., Brown, A. S., and Stockwell, P. B.: Elemental mercury vapour in air: the origins and validation of the 'Dumarey equation' describing the mass concentration at saturation, Accredit. Qual. Assur., 15, 409–414, https://doi.org/10.1007/s00769-010-0645-1, 2010.

Dunham-Cheatham, S. M., Lyman, S., and Gustin, M. S.: Evaluation of sorption surface materials for reactive mercury compounds, Atmos. Environ., 242, 117836, https://doi.org/10.1016/j.atmosenv.2020.117836, 2020.

Dunham-Cheatham, S. M., Lyman, S., and Gustin, M. S.: Comparison and calibration of methods for ambient reactive mercury quantification, Sci. Total Environ., 856, 159219, https://doi.org/10.1016/j.scitotenv.2022.159219, 2023.

Elgiar, T.R., Lyman, S.N., Andron, T.D., Gratz, L., Hallar, A.G., Horvat, M., Vijayakumaran Nair, S., O'Neil, T., Volkamer, R. and Živković, I.: Traceable Calibration of Atmospheric Oxidized Mercury Measurements, Environ. Sci. Technol., 58, 10706-10716, https://doi.org/10.1021/acs.est.4c02209, 2024.

Gačnik, J., Lyman, S. N., Dunham-Cheatham, S. M., and Gustin, M. S.: Limitations and insights regarding atmospheric mercury sampling using gold, Anal Chim Acta, 1319, 342956, https://doi.org/10.1016/j.aca.2024.342956, 2024.

Gačnik, J., Živković, I., Ribeiro, S.G., Kotnik, J., Berisha, S., Nair, S.V., Jurov, A., Cvelbar, U. and Horvat, M.: Calibration approach for gaseous oxidized mercury based on nonthermal plasma oxidation of elemental mercury, Anal. Chem., 94, 8234-8240, https://doi.org/10.1021/acs.analchem.2c00260, 2022

Gustin, M. S., Dunham-Cheatham, S. M., Allen, N., Choma, N., Johnson, W., Lopez, S., Russell, A., Mei, E., Magand, O., Dommergue, A., and Elgiar, T.: Observations of the chemistry and concentrations of reactive Hg at locations with different ambient air chemistry, Sci. Total Environ., 904, 166184, https://doi.org/10.1016/j.scitotenv.2023.166184, 2023.

Gustin, M. S., Dunham-Cheatham, S. M., and Zhang, L.: Comparison of 4 methods for measurement of reactive, gaseous oxidized, and particulate bound mercury, Environ. Sci. Technol., 53, 14489-14495, https://doi.org/10.1021/acs.est.9b04648, 2019.

Gustin, M. S., Dunham-Cheatham, S. M., Zhang, L., Lyman, S., Choma, N., and Castro, M.: Use of membranes and detailed HYSPLIT analyses to understand atmospheric particulate, gaseous oxidized, and reactive mercury chemistry, Environ. Sci. Technol., 55, 893-901, https://doi.org/10.1021/acs.est.0c07876, 2021.

Holmes, C.D., Jacob, D.J., Corbitt, E.S., Mao, J., Yang, X., Talbot, R. and Slemr, F.: Global atmospheric model for mercury including oxidation by bromine atoms, Atmos. Chem. Phys., 10, 12037-12057, https://doi.org/10.5194/acp-10-12037-2010, 2010.

Horowitz, H.M., Jacob, D.J., Zhang, Y., Dibble, T.S., Slemr, F., Amos, H.M., Schmidt, J.A., Corbitt, E.S., Marais, E.A. and Sunderland, E.M.: A new mechanism for atmospheric mercury redox chemistry: implications for the global mercury budget, Atmos. Chem. Phys., 17, 6353-6371, https://doi.org/10.5194/acp-17-6353-2017, 2017.

Huang, J. and Gustin, M. S.: Uncertainties of gaseous oxidized mercury measurements using KCl-coated denuders, cation-exchange membranes, and nylon membranes: humidity influences, Environ. Sci. Technol., 49, 6102–6108, https://doi.org/10.1021/acs.est.5b00098, 2015.

Huang, J., Miller, M. B., Weiss-Penzias, P., and Gustin, M. S.: Comparison of gaseous oxidized Hg measured by KCl-coated denuders, and nylon and cation exchange membranes, Environ. Sci. Technol., 47, 7307–7316, https://doi.org/10.1021/es4012349, 2013.

Jones, C. P., Lyman, S. N., Jaffe, D. A., Allen, T., and O'Neil, T. L.: Detection and quantification of gas-phase oxidized mercury compounds by GC/MS, Atmos. Meas. Tech., 9, 2195-2205, https://doi.org/10.5194/amt-9-2195-2016, 2016.

Kaulfus, A. S., Nair, U., Holmes, C. D., and Landing, W. M.: Mercury wet scavenging and deposition differences by precipitation type, Environ. Sci. Technol., 51, 2628–2634, https://doi.org/10.1021/acs.est.6b04187, 2017.

Khalizov, A.F., Guzman, F.J., Cooper, M., Mao, N., Antley, J. and Bozzelli, J.: Direct detection of gas-phase mercuric chloride by ion drift-chemical ionization mass spectrometry, Atmos. Environ., 238, 117687, https://doi.org/10.1016/j.atmosenv.2020.117687, 2020.

Landis, M. S., Stevens, R. K., Schaedlich, F., and Prestbo, E. M.: Development and characterization of an annular denuder methodology for the measurement of divalent inorganic reactive gaseous mercury in ambient air, Environ. Sci. Technol., 36, 3000-3009, https://doi.org/10.1021/es015887t, 2002.

Laurier, F.J., Mason, R.P., Whalin, L. and Kato, S.: Reactive gaseous mercury formation in the North Pacific Ocean's marine boundary layer: A potential role of halogen chemistry, J. Geophys. Res-Atmos., 108, 4529, https://doi.org/10.1029/2003JD003625, 2003.

Luippold, A., Gustin, M. S., Dunham-Cheatham, S. M., Castro, M., Luke, W., Lyman, S., and Zhang, L.: Use of multiple lines of evidence to understand reactive mercury concentrations and chemistry in Hawai'i, Nevada, Maryland, and Utah, USA, Environ. Sci. Technol., https://doi.org/10.1021/acs.est.0c02283, 54, 7922-7931. 2020a

Luippold, A., Gustin, M. S., Dunham-Cheatham, S. M., and Zhang, L.: Improvement of quantification and identification of atmospheric reactive mercury, Atmos. Environ., 224, 117307, https://doi.org/10.1016/j.atmosenv.2020.117307, 2020b.

Lyman, S. N., Cheng, I., Gratz, L. E., Weiss-Penzias, P., and Zhang, L.: An updated review of atmospheric mercury, Sci. Total Environ., 707, 135575, https://doi.org/10.1016/j.scitotenv.2019.135575, 2020a.

Lyman, S. N., Gratz, L. E., Dunham-Cheatham, S. M., Gustin, M. S., and Luippold, A.: Improvements to the accuracy of atmospheric oxidized mercury measurements, Environ. Sci. Technol., 54, 13379–13388, https://doi.org/10.1021/acs.est.0c02747, 2020b.

Lyman, S. N., and Jaffe, D. A.: Formation and fate of oxidized mercury in the upper troposphere and lower stratosphere. Nat. Geosci., 5, 114-117, https://doi.org/10.1038/ngeo1353, 2012.

Lyman, S., Jones, C., O'Neil, T., Allen, T., Miller, M., Gustin, M.S., Pierce, A.M., Luke, W., Ren, X. and Kelley, P.: Automated calibration of atmospheric oxidized mercury measurements, Environ. Sci. Tech., 50, 12921-12927, https://doi.org/10.1021/acs.est.6b04211, 2016.

Manos, M. J. and Kanatzidis, M. G.: Metal sulfide ion exchangers: superior sorbents for the capture of toxic and nuclear waste-related metal ions, Chem. Sci., 7, 4804–4824, https://doi.org/10.1039/C6SC01039C, 2016.

Mao, N. and Khalizov, A.: Exchange reactions alter molecular speciation of gaseous oxidized mercury, ACS Earth Space Chemistry, 5, 1842–1853, https://doi.org/10.1021/acsearthspacechem.1c00178, 2021.

McClure, C. D., Jaffe, D. A., and Edgerton, E. S.: Evaluation of the KCl denuder method for gaseous oxidized mercury using $HgBr_2$ at an in-service AMNet Site, Environ. Sci. Technol., 48, 11437–11444, https://doi.org/10.1021/es502545k, 2014.

Miller, M.B., Dunham-Cheatham, S.M., Gustin, M.S. and Edwards, G.C.: Evaluation of cation exchange membrane performance under exposure to high Hg^0 and $HgBr_2$ concentrations, Atmos. Meas. Tech., 12, 1207-1217, https://doi.org/10.5194/amt-12-1207-2019, 2019.

R Core Team: _R: A language and environment for statistical computing_, https://www.R-project.org/, 2023.

Shah, V., Jacob, D. J., Thackray, C. P., Wang, X., Sunderland, E. M., Dibble, T. S., Saiz-Lopez, A., Černušák, I., Kellö, V., Castro, P. J., Wu, R., and Wang, C.: Improved mechanistic model of the atmospheric redox chemistry of mercury, Environ. Sci. Technol., 55, 14445–14456, https://doi.org/10.1021/acs.est.1c03160, 2021.

Song, Z., Huang, S., Zhang, P., Yuan, T. and Zhang, Y.: Isotope Data Constrains Redox Chemistry of Atmospheric Mercury, Environ. Sci. Tech., 58, 13307-13317, https://doi.org/10.1021/acs.est.4c02600, 2024.

Steffen, A., Douglas, T., Amyot, M., Ariya, P., Aspmo, K., Berg, T., Bottenheim, J., Brooks, S., Cobbett, F., Dastoor, A. and Dommergue, A.: A synthesis of atmospheric mercury depletion event chemistry in the atmosphere and snow, Atmos. Chem. Phys., 8, 1445-1482, https://doi.org/10.5194/acp-8-1445-2008, 2008.

Szymańska, E. and Winnicka, K.: Stability of chitosan—a challenge for pharmaceutical and biomedical applications, Mar. Drugs, 13, 1819–1846, https://doi.org/10.3390/md13041819, 2015.

United States Environmental Protection Agency: Method 1631, Revision E: Mercury in water by oxidation, purge and trap, and cold vapor atomic fluorescence spectrometry, 2002.

United States Environmental Protection Agency: Appendix to Method 1631, Total mercury in tissue, sludge, sediment, and soil by acid digestion and BrCl oxidation, 2001.

United States Environmental Protection Agency: Method 3052, Revision 0: Microwave assisted acid digestion of siliceous and organically based matrices, EPA publication SW-846, 1996.

United States Environmental Protection Agency: Method 7473, Revision 0: Mercury in Solids and Solutions by thermal decomposition, amalgamation, and atomic absorption spectrophotometry, EPA publication SW-846, 2007.

Vieira, R. S. and Beppu, M. M.: Interaction of natural and crosslinked chitosan membranes with Hg(II) ions, Colloid Surface A, 279, 196–207, https://doi.org/10.1016/j.colsurfa.2006.01.026, 2006.

Western Regional Climate Center: https://raws.dri.edu/, last access: 2 February 2024.

Yu, J. G., Yue, B. Y., Wu, X. W., Liu, Q., Jiao, F. P., Jiang, X. Y., and Chen, X. Q.: Removal of mercury by adsorption: a review, Environ. Sci. Pollut. R., 23, 5056–5076, https://doi.org/10.1007/s11356-015-5880-x, 2016.

Zheng, Y., Duan, Y., Tang, H., Li, C., Li, J., Zhu, C., and Liu, S.: Experimental research on selective adsorption of gaseous mercury (II) over SiO2, TiO2 and γ-Al2O3, Fuel, 237, 202–208, https://doi.org/10.1016/j.fuel.2018.09.153, 2019.

Zimmermann, T., Von Der Au, M., Reese, A., Klein, O., Hildebrandt, L., and Pröfrock, D.: Substituting HF by HBF_4 – an optimized digestion method for multi-elemental sediment analysis via ICP-MS/MS, Anal. Methods-UK, 12, 3778–3787, https://doi.org/10.1039/D0AY01049A, 2020.

Formatted: Superscript

Formatted: Subscript